

## Powder characteristics of Fe<sub>2</sub>O<sub>3</sub> nanopowder agglomerates fabricated by high energy ball milling at various speed and spray-drying processes

Jun-Il Song, Geon-Yong Lee, Jong-ryoul Kim and Jai-Sung Lee\*

Department of Materials Science and Chemical Engineering, Hanyang University-ERICA, Ansan 15588, Korea

This study investigated the effects of milling speed on the structure evolution of spray-dried (SD) Fe<sub>2</sub>O<sub>3</sub> agglomerate as a precursor for fabricating Fe nanopowder agglomerate. For fabrication, the milling speed was controlled at four different rotation speeds of 1000, 1400, 1800 and 2400 rpm (revolution per minute) for 10 hrs. For quantitative analysis, a microstructural observation was conducted. The particle size first decreased rapidly until it finally reached a saturation value of about 60 nm as the milling rpm increased to 1800 rpm. Moreover, it was found that excessive milling energy was consumed to form secondary agglomerates in spherical agglomerate at milling condition of 2400 rpm. The evolution of powder characteristics is also discussed in terms of the crystallite size and surface area and then compared to the particle size distribution analyzed by the microstructure.

**Key words** Fe<sub>2</sub>O<sub>3</sub> nanopowder, Spherical agglomerate, Bead milling, Particle size distribution, Crystallite size.

### Introduction

The potential application of nanocrystalline materials utilized in structural applications largely depends on the consolidation of powders into bulk nanoscale solids [1-3]. The full-densification with uniform microstructure is a primary concern for preserving the superior mechanical properties of the material [4, 5]. Among the various approaches to fabricate metal nanopowder, the mechano-chemical process which is the mechanical ball milling of metal oxide powder and subsequent hydrogen reduction of the chemical process, is one of the most promising routes [6, 7]. The use of the metal oxide powder as a starting material is easy to reduce particle size down to nanometer size owing to the brittleness of the metal oxide particles in the ceramic phase [8, 9]. Furthermore, hydrogen reduction of oxide powder is well known for advantageous process in terms of cost-effectiveness, environment-friendliness, and ease of structural design [9, 10].

Recently the authors reported that the spherical shaped iron agglomerate powder consisting of bimodal structured Fe nanoparticles can be fabricated by the controlled hydrogen reduction process of spray-dried (SD) iron oxide nanopowder agglomerates [11]. It was also found that the bimodal iron nanopowder agglomerates interestingly have an excellent compactability over 70% theoretical density at conventional compaction conditions.

This bimodality of the powder structure is basically responsible for improvement of the compaction property by increasing the packing density. In this respect, it is very important to understand how the bimodal agglomerate structure is formed in the entire powder making processes including oxide-milling, spray-drying, and hydrogen reduction in order to optimize the processing conditions. Among the many processing parameters, the initial structure parameters of SD iron oxide nanopowder agglomerates such as nanoparticle size and distribution, pore volume and size distribution are firstly presumed to initiate such bimodal structure evolution of Fe nanopowder during the reduction process. This is because the agglomerate structure plays a decisive role in controlling the hydrogen reduction process thermodynamically as well as kinetically, as a determining the structure of iron agglomerate powder [6].

The tool chosen for changing the agglomerate structure of iron oxide in this study, is the control of milling energy by varying milling speed. Several investigations of the milling energy effect controlled by milling speed and time have been reported [12-14]. According to Arbain et al. [15], the increase of milling speed resulted in decrease of the crystallite size of hematite up to about 20 nm. Sanchez et al. [16] also prolonged the milling time, which resulted in a decrease in the particle size of hematite up to about 30 nm. Such milling energy effect was interpreted in terms of excess energy generated during milling. When particle refinement by milling is ended, the excess collision energy due to prolonged milling is spent on formation of the primary particle agglomeration [16-18]. This result points out that such primary agglomeration

\*Corresponding author:  
Tel : +82-400-5225  
Fax: +82-406-5170  
E-mail: jslee@hanyang.ac.kr

of oxide nanoparticles presumably acts as the initiator of further bimodal particle growth during the reduction process.

Another unavoidable factor affecting particle agglomeration is the drying process in the case of wet-milling due to van der Waals or other attraction force [19, 20]. The interparticle attractive force causes the agglomerate to have an irregular shape and broad size distribution during the drying process. Strong and irregular shaped agglomerates, which do not break down during pressing, reduce the achievable packing density and produce compacts with non-uniform pore size distribution in which the coarser pores may remain in the sintered body [21, 22]. To prevent this phenomenon, some ceramic powders are intentionally agglomerated in a spherical form by spray drying process to enhance their flowability and handling [23]. Among the spray-drying processes, binderless spray-drying is widely used to fabricate spherical agglomerate with weak agglomeration strength to be easily broken during compaction [20]. This process can enhance not only the uniformity of agglomerate with a spherical shape and uniform size but also the particle rearrangement during compaction due to the weak agglomeration strength [21, 24].

Based upon the previous reports as described above, the present study attempted to investigate the effect of milling speed on the structure evolution in spray-dried  $\text{Fe}_2\text{O}_3$  agglomerate powders as the first part of a study for fabrication microstructure-optimized spherical shaped Fe nanopowder agglomerates with improved compactability. For this purpose, we examine the evolution of powder characteristics depending on milling speed and then discuss the correlation between the characteristics of as-milled precursor powder and those of the SD agglomerates.

## Experimental Procedure

In this study, commercially available  $\alpha\text{-Fe}_2\text{O}_3$  powders (Kojundo Chemical, 99.9%, 1  $\mu\text{m}$  in average size, Fig. 1) were used as a raw material which was ball-milled and spray-dried in order to fabricate  $\text{Fe}_2\text{O}_3$  nanopowder agglomerate.

The ball-milling was conducted by bead milling system (Ultra bead mill, Nanointech Inc., Korea) in methyl alcohol with steel beads (1 mm in diameter). In this process, we selected four different milling speeds of 1000, 1400, 1800 and 2400 rpm (revolution per minute) for 10 h. The main experimental variable of milling speed in this study was chosen for the purpose of inducing the structural change of  $\text{Fe}_2\text{O}_3$  nanopowder. After the ball-milling process, the obtained slurries were spray-dried using small sized spray dryer (MH-8, Mehyun Engineering Inc., Korea) with optimized condition of feeding rate of 2500 cc/hr into spray drier, inlet air pressure of 80 kPa and inlet temperature at 30 °C. The fine agglomerates of the  $\alpha\text{-Fe}_2\text{O}_3$  nanopowder collected by the cyclone, and the coarse granules

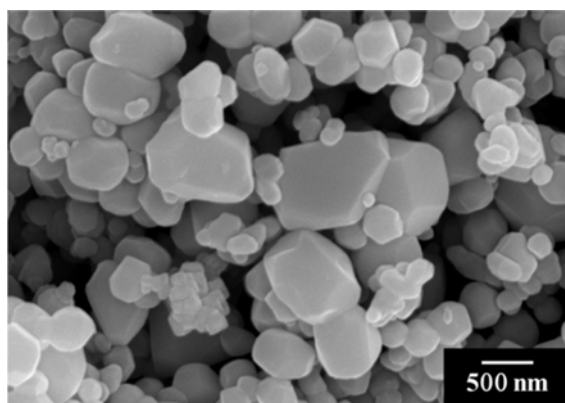


Fig. 1. SEM micrograph of  $\alpha\text{-Fe}_2\text{O}_3$  powder as raw material.

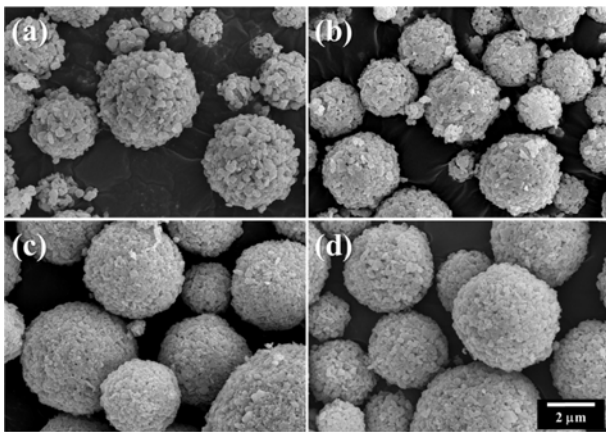
collected in the main chamber were discarded [6]. They were dried at 70 °C for 12 h and then, sieved down to particle diameter of 150  $\mu\text{m}$  (sieve size, 100 mesh).

In order to investigate the microstructural development of powders during the process, the fabricated powders in each step of the as-milled and spray-dried (SD) were observed by field emission scanning electron microscope (FE-SEM, Hitachi S-4800, Japan). The particle size distribution analysis was conducted by counting at least 2000 randomly selected particles from SEM micrographs of the powders. To determine particle size, the Feret diameter,  $D_f$ , which is the distance between the pairs of parallel tangents to the projected outline of the particle in a fixed direction, was used in assuming that the particles are in random orientation [25]. Also, the mean crystallite size and surface area of the SD powders were investigated by indirect analysis methods. The mean crystallite size was calculated using Scherrer's formula from a X-ray diffraction analysis (XRD, Rigaku D/MAX-2500/PC) using Cu  $K\alpha$  radiation ( $\lambda = 0.15406$  nm) as a target [26], and the surface area was measured by a Brunauer-Emmett-Teller analysis (BET, ATI Autosorb-1, USA) using nitrogen adsorption method [25].

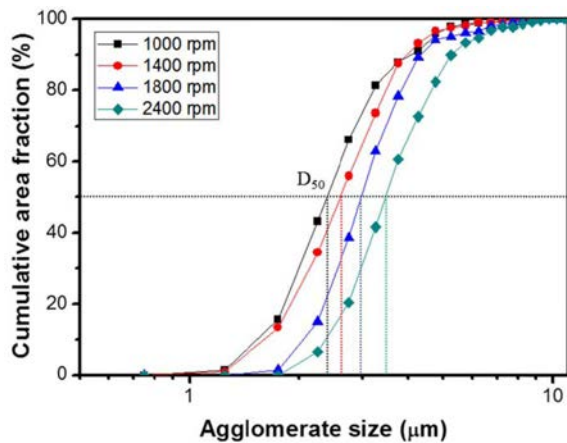
## Results and Discussion

Fig. 2 shows the SEM micrographs of the SD  $\text{Fe}_2\text{O}_3$  nanopowder agglomerates which were prepared under milling speed conditions of 1000, 1400, 1800, and 2400 rpm, respectively. It is apparent that all powder samples have a spherical agglomerate shape ranging from 1-5  $\mu\text{m}$  in size consisting of various sized  $\text{Fe}_2\text{O}_3$  fine particles. At a low milling speed below 1400 rpm, however, the agglomerate powders have a relatively smaller size and rougher surface compared to those of higher speed conditions over 1800 rpm.

This macroscopic observation of the agglomerates was quantitatively examined by measurement of the size distribution of the agglomerates as shown in Fig. 3. As seen in the result, the SD agglomerate size increased with increasing milling speed in a range from 1-5  $\mu\text{m}$



**Fig. 2.** SEM micrographs of SD Fe<sub>2</sub>O<sub>3</sub> nanopowder agglomerates at various milling speed (rpm): (a) 1000, (b) 1400, (c) 1800, and (d) 2400.



**Fig. 3.** The cumulative agglomerate size distributions in SD Fe<sub>2</sub>O<sub>3</sub> nanopowder agglomerates at various milling speed.

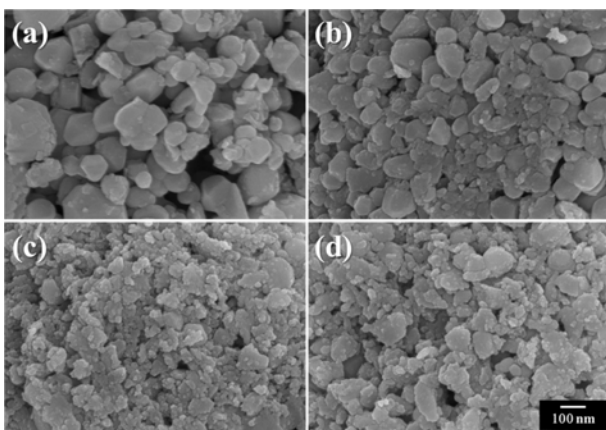


**Fig. 4.** Surface microstructures of SD Fe<sub>2</sub>O<sub>3</sub> nanopowder agglomerates at various milling speed (rpm): (a) 1000, (b) 1400, (c) 1800, and (d) 2400.

as described above.

Fig. 4 shows the microstructure of Fe<sub>2</sub>O<sub>3</sub> particles inside the agglomerates at higher magnification images. It is confirmed that milling speed affects the structure of Fe<sub>2</sub>O<sub>3</sub> particles considerably. With increasing milling

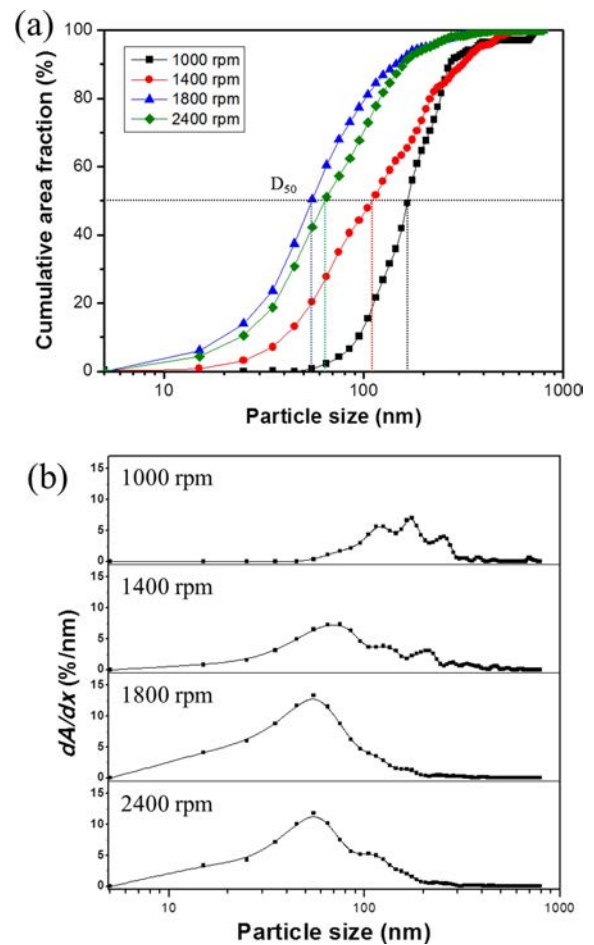


**Fig. 5.** Particle size distributions in SD Fe<sub>2</sub>O<sub>3</sub> nanopowder agglomerates at various milling speed: (a) cumulative area fraction curve and (b) differential cumulative area fraction curve.

speed, the Fe<sub>2</sub>O<sub>3</sub> particles became smaller, particularly at the 1800 rpm condition. However, the more powerful milling at 2400 rpm resulted in a slightly coarsened Fe<sub>2</sub>O<sub>3</sub> particle microstructure. Such a difference in the agglomerate structure is basically thought to originate from the different cohesion forces between the primary particles. It is well known that the cohesion force forming agglomerates is in an inverse linear relationship with the particle size [19, 20] and the agglomerates of small particles are more stable in contrast to those of large particles. In addition, it should be noted that some Fe<sub>2</sub>O<sub>3</sub> particles in the agglomerates partly underwent a shape change from polyhedral (see Fig. 1) to angular type during the milling process. This change results from the brittle fracture of oxide particles by mechanical milling [16, 27].

The microstructural observation in the result of Fig. 4 can be discussed by quantitative analysis and calculation of the microstructure. Fig. 5 represents the result for the cumulative particle size distribution of the SD Fe<sub>2</sub>O<sub>3</sub> nanopowder agglomerates prepared at various milling speed. It is noted that the cumulative frequency value of the particle size was evaluated in

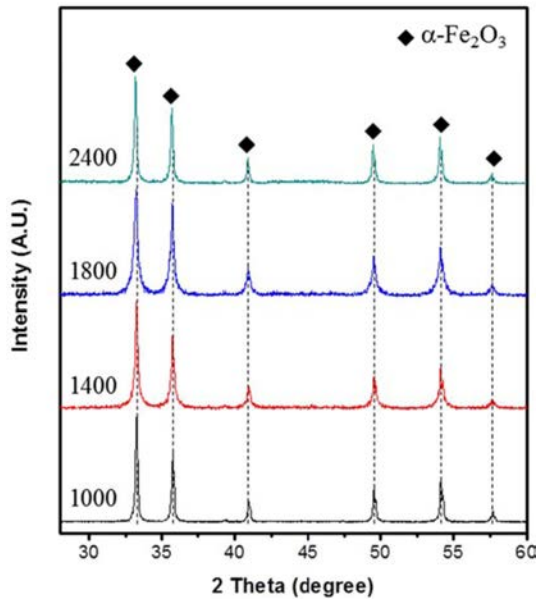


**Fig. 6.** The X-ray diffraction patterns of SD  $\text{Fe}_2\text{O}_3$  nanopowder agglomerates at various milling speed (rpm): (a) 1000, (b) 1400, (c) 1800, and (d) 2400.

terms of particle area by the following Eq. (1):

$$A = \frac{\pi}{4} D_f^2 \quad (1)$$

where  $A$  is the area of identical spherical particle and is calculated using the measured particle size, Feret diameter,  $D_f$ . By adding the interval percentages of the calculated area with respect to all the measured particles, the cumulative frequency value of the particle size of Fig. 5(a) was obtained.

As can be seen in Fig. 5(a), the cumulative area fraction distribution curves are shifted to a lower particle size range with increasing milling speed. However, it was also found that the higher milling speed condition at 2400 rpm resulted in a shift of the size distribution to more or less higher size range compared to the case of 1800 rpm. Namely, with increasing milling speed the particle size gradually decreases until it reaches a minimum value and then remains unchanged or becomes slightly larger even at much higher milling conditions. This result on the relationship between particle size distribution and milling speed is consistent with that of microstructure development as described above in Fig. 4. Moreover, it can be more exactly explained by examining the variation of differential cumulative size distribution curve as a function of the milling speed. The differential cumulative distribution can be calculated from the slope,  $dA/dx$  of the cumulative curve at particle size  $x$  according to Eq. (2):

$$A(x_2) - A(x_1) = \int_{x_1}^{x_2} \frac{dA}{dx} \cdot dx \quad (2)$$

The area  $A$  under the curve between two particle sizes

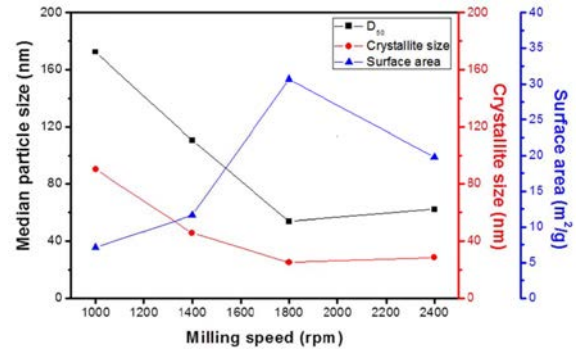


**Fig. 7.** Variations of median particle size, crystallite size, and surface area of SD  $\text{Fe}_2\text{O}_3$  nanopowder agglomerates with increasing milling speed.

**Table 1.** The results of the powder characteristics of SD  $\text{Fe}_2\text{O}_3$  nanopowder agglomerates at various milling speed conditions.

Milling speed (rpm)	1000	1400	1800	2400
$D_{50}$ (nm)	172.6	110.5	53.8	62.1
Crystallite size (nm)	90.2	45.7	25.0	28.3
Surface area ( $\text{m}^2/\text{g}$ )	7.14	11.61	30.69	19.76

(i.e.,  $x_1$  and  $x_2$ ) indicates the occupying area of the particles whose diameters are comprised in that interval [25, 28]. Then,  $dA/dx$ , the slope of the curve at particle size  $x$  corresponds to the area frequency at this size.

Fig. 5(b) shows the differential cumulative distribution curves depending on the logarithmic particle size, which was calculated based on Eq. (2) for various milling speed conditions. As seen in the results, the highest peak in the differential distribution curve indicating the mode diameter apparently moved toward smaller size range as the milling speed increased up to 1800 rpm. It was also found that the highest peak of the 2400 rpm sample took place at the same particle size as the 1800 rpm sample. This indicates that the mode diameter values of both samples of 1800 and 2400 rpm are equal to be about 50 nm. However, there is a secondary peak at larger particle size of 120 nm in the 2400 rpm sample.

This suggests that mechanical milling for particle refinement has limits and rather seems to make some strong agglomerates of small size. In order to verify this, the results of SEM image analysis were compared with the crystallite size and gas adsorption surface area by XRD and BET measurements. The former value of crystallite size was calculated by the Scherrer formula [26] based on X-ray diffraction patterns. Fig. 6 represents the results of X-ray diffraction patterns for four SD iron oxide agglomerate powders. During the milling and spray-drying process, the contamination is not found with increasing milling speed. Moreover, it is seen that with increasing milling speed, the main XRD peaks underwent a line broadening, which is basically due to particle refinement. The data of the average

crystallite size calculated based on the line broadening of the X-ray peaks are listed in Table 1 together with the data of median particle size ( $D_{50}$ , 50% size on the cumulative curve) and surface area for comparison. In particular, all these data are represented as a function of the milling speed in Fig. 7.

As can be seen in Fig. 7, both particle sizes,  $D_{50}$  and the crystallite size of the powders show a very similar behavior in dependence of milling speed in which the increasing milling speed both sizes rapidly decreased until the milling speed reached 1800 rpm and afterwards increased slightly up to 2400 rpm. However, the size values were not equal where the particle size was approximately two times larger than the crystallite size during the entire milling speed conditions. The calculated crystallite size decreased to a saturation size of about 30 nm at 1800 rpm. In contrast, the surface area of the powders showed an opposite behavior against the particle size. It abruptly increased to 30 m<sup>2</sup>/g up to 1800 rpm and then gradually decreased to 20 m<sup>2</sup>/g at 2400 rpm.

The experimental results of Fig. 7 can be interpreted based upon the previous literature as follows. It is well known that the milling energy on the powder is consumed to break interatomic bonds in the crystal and to create additional surface as a result of the cleavage of crystalline grains [27, 29]. However, particle refinement by mechanical milling is limited at a certain milling speed and even higher conditions. This result can be interpreted in terms of the particle size and applied pressure. As the particle size of the powder decreases by milling, the compressive stress from the collision energy is below the fracture strength of the particles since the fracture strength of the brittle materials varies inversely with the size [16].

The present study clearly shows that the milling condition of 1800 rpm yields the finest particle and crystallite size with the largest surface area. Moreover, the prolonged collision energy after the milling at 1800 rpm is spent by friction energy via sliding of nanoparticles past each other followed by coalescence to form strong agglomeration in a slurry [16, 17]. These results might be related to the evolution of bimodal particle growth during hydrogen reduction. Namely, it is considered that the milling condition of 1800 rpm provides an optimal condition for the bimodal structure in terms of thermodynamic and kinetic of the reaction during hydrogen reduction process. This issue will be discussed in further work.

## Conclusions

The present study attempted to investigate the effects of milling speed on the structure evolution in spray-dried (SD) Fe<sub>2</sub>O<sub>3</sub> agglomerate powders as the first part of a study for fabrication microstructure-optimized spherical shaped Fe nanopowder agglomerates. With

increasing milling energy, the primary particle size was decreased and then saturated to 60 nm over 1800 rpm. Moreover, it was found that excessive milling energy was consumed to form secondary agglomerates of 140 nm in spherical agglomerate. This observed result agrees with the crystallite size calculated from the XRD data and surface area analyzed by BET. The crystallite size was decreased and saturated about 30 nm until the milling speed reached 1800 rpm and afterwards increased slightly up to 2400 rpm. Moreover, the surface area of powders abruptly increased to 30 m<sup>2</sup>/g up to 1800 rpm and then gradually decreased to 20 m<sup>2</sup>/g at 2400 rpm. It means that the mechanical milling for particle refinement has limits and seems to create some strong secondary agglomerates. Based on these results, it may be related to bimodal particle growth during hydrogen reduction. In the near future, correlation of milling effect and bimodal particle growth will be reported by using the precursor of SD Fe<sub>2</sub>O<sub>3</sub> nanopowder agglomerates.

## Acknowledgments

This work was supported by the Human Resources Development Program (No. 20174030201830) of the Korea Institute of Energy Technology Evaluation and Planning (KETEP) grant funded by the Korea government Ministry of Trade, Industry and Energy.

## References

1. J.-S. Lee, J.-P. Choi, G.-Y. Lee, *Materials* 6 (2013) 4046-4063.
2. D. Zhang, *Prog. Mater. Sci.* 49 (2004) 537-560.
3. P. Bowen, C. Carry, *Powder Technol.* 128 (2002) 248-255.
4. C. Chen, Z. Ding, Q. Tan, H. Qi, Y. He, *Powder Technol.* 257 (2014) 83-87.
5. J.R. Groza, *Nanostruct. Mater.* (2007) 173-217.
6. G.-Y. Lee, J.-I. Song, J.-S. Lee, *Powder Technol.* 302 (2016) 215-221.
7. S.-S. Ryu, H.-R. Park, Y.-D. Kim, H.-S. Hong, *Int. J. Refract. Met. Hard Mater.* (2016).
8. G. Hahn, *Metall. Mater. Trans. A* 15 (1984) 947-959.
9. G.-Y. Lee, J.-P. Choi, J.-I. Song, S.-S. Jung, J.-S. Lee, *Mater. Trans.* 55 (2014) 1611-1617.
10. P. Pourghahramani, E. Forsberg, *Thermochim. Acta* 454 (2007) 69-77.
11. G.-Y. Lee, in "A Thesis for the Degree of Doctor of philosophy", (Hanyang University Press, 2016) p. 45.
12. S. Mende, F. Stenger, W. Peukert, J. Schwedes, *Powder Technol.* 132 (2003) 64-73.
13. S. Hennart, M. Domingues, W. Wildeboer, P. Van Hee, G. Meesters, *Powder Technol.* 198 (2010) 56-60.
14. O. Celep, N. Aslan, İ. Alp, G. Taşdemir, *Powder Technol.* 208 (2011) 121-127.
15. R. Arbain, M. Othman, S. Palaniandy, *Miner. Eng.* 24 (2011) 1-9.
16. C.A. Galan, A.L. Ortiz, F. Guiberteau, L.L. Shaw, *J. Am. Ceram. Soc.* 92 (2009) 3114-3117.
17. A.K. Nath, C. Jiten, K.C. Singh, *Physica B* 405 (2010) 430-434.
18. N. Traiphol, *J. Ceram. Process. Res.* 8 (2007) 137-141.

19. R.Y. Yang, A.B. Yu, S.K. Choi, M.S. Coates, H.K. Chan, Powder Technol. 184 (2008) 122-129.
20. M. Horio, Powder Technol. 130 (2003) 1-7.
21. M. Ciftcioglu, M. Akinc, L. Burkhart, J. Am. Ceram. Soc. 70 (1987) C-329-C-334.
22. B.J. Briscoe, N. Özkan, Powder Technol. 90 (1997) 195-203.
23. S. Cottrino, Y. Jorand, J. Adrien, C. Olagnon, Powder Technol. 237 (2013) 586-593.
24. S.J. Lukasiewicz, J. Am. Ceram. Soc. 72 (1989) 617-624.
25. T. Allen, in "Particle Size Measurement", (Springer, 2013) p. 138.
26. B.D. Cullity, S.R. Stock, in "Elements of X-ray Diffraction, Prentice hall Upper Saddle River", (Addison-Wesley Publishing Compony, Inc., 2001) p. 170.
27. Y. Waseda, A. Muramatsu, in "Morphology control of materials and nanoparticles: advanced materials processing and characterization", (Springer Science & Business Media, 2003) p. 94.
28. A. Macias-Garcia, E.M. Cuerda-Correa, M. Diaz-Diez, Mater. Charact. 52 (2004) 159-164.
29. A. Gusev, A. Kurlov, Nanotechnol. 19 (2008) 265302-265309.